Hot pressing of Yb:Y_2O_3 laser ceramics with LiF sintering aid

Stanislav Balabanov[a,*], Dmitry Permin[a], Timofey Evstropov[a], Pavel Andreev[a], Liza Basyrova[b], Patrice Camy[b], Mikhail Baranov[c], Xavier Mateos[d,e], and Pavel Loiko[b]

[a]*G.G. Devyatykh Institute of Chemistry of High-Purity Substances of the RAS, Nizhny Novgorod, Russia*
[b]*Centre de recherche sur les Ions, les Matériaux et la Photonique (CIMAP), UMR 6252 CEA-CNRS-ENSICAEN, Université de Caen, 6 Boulevard du Maréchal Juin, 14050 Caen, France*
[c]*ITMO University, Kronverkskiy Pr., 49, 197101 Saint-Petersburg, Russia*
[d]*Universitat Rovira i Virgili (URV), Física i Cristal·lografia de Materials i Nanomaterials (FiCMA-FiCNA)-EMaS, Marcel·lí Domingo 1, 43007 Tarragona, Spain*
[e]*Serra Húnter Fellow*
**Corresponding author, e-mail: balabanov@ihps-nnov.ru*

Abstract: Transparent ytterbium-doped yttria ceramics, 2 at.% Yb:Y_2O_3, were fabricated by hot uniaxial pressing in vacuum at 1550 °C / 50 MPa followed by a two-stage Hot Isostatic Pressing (HIPing) at 1200 - 1400 °C / 100 MPa, using nanopowders obtained by self-propagating high-temperature synthesis (with lithium fluoride serving as a sintering aid). The addition of LiF during the powder synthesis markedly changed the morphology of powders, and at the stage of hot pressing, drastically reduced the carbon contamination of ceramics, as well as stimulated sintering without formation of the liquid phase. The spectroscopic properties of ceramics were studied. The stimulated-emission cross-section for Yb^{3+} ions is 0.90×10^{-20} cm^2 at 1030.4 nm and the luminescence lifetime is 797 μs. A continuous-wave 2 at.% Yb:Y_2O_3 ceramic laser generated an output power of 735 mW at 1027-1034 nm with a slope efficiency of 64.5% and a laser threshold of 0.28 W.

Keywords: transparent ceramics; sintering aid; yttrium oxide; ytterbium ion; luminescence; laser operation.

1. Introduction

Transparent polycrystalline ceramic based on cubic (C-type, bixbyite structure) yttrium sesquioxide (yttria, Y_2O_3) doped with ytterbium (Yb^{3+}) ions is an attractive laser gain medium. The host matrix exhibits good thermo-mechanical properties such as high thermal conductivity (κ = 12.8 $Wm^{-1}K^{-1}$ at 300 K), suitable hardness and weak thermal expansion and it can be easily doped with Yb^{3+} ions. The raw reagents needed for the ceramic production are relatively cheap (as compared, e.g., to other sesquioxide ceramics based on Lu_2O_3 or Sc_2O_3). The research on Yb:Y_2O_3 laser ceramics was stimulated by the pioneering work of Lu *et al*. [1]. Since then, different methods of fabrication of ceramics based on Y_2O_3 were proposed, i.e., vacuum synthesis [2], hot pressing [3], spark plasma synthesis (SPS) [4], self-propagating high-temperature synthesis [5], etc. The main difficulty for obtaining high optical quality Yb:Y_2O_3 ceramic (similarly to other cubic sesquioxides) is the strong competition of processes of densification and grain growth. This leads to pore trapping in the volume of the grains, formation of pores at triple points and grain boundaries and, consequently, to strong light scattering.

The densification of ceramics at the intermediate and final stages of the synthesis can be promoted by using various sintering aids. Among them, the most efficient (for achieving full ceramic density) and widely used ones for the synthesis of Y_2O_3 are ZrO_2 and HfO_2 [6,7]. Their disadvantages for laser applications are the possible change of the valence state of Zr and Hf under laser irradiation and formation of free carriers leading to degradation of the optical properties of the ceramics [8]. Another efficient sintering aid is La_2O_3. The introduction of about 10 mol% La_2O_3 notably promotes the diffusion of ions [9,10] leading to the fabrication of Yb:Y_2O_3 laser ceramics [11]. As compared to ceramics with heterovalent sintering aids, such materials do not exhibit degradation of their laser properties with time. On the other hand, the addition of La_2O_3 leads to a sharp decrease of the thermal conductivity of the ceramics. Even more effective for achieving optical transparency of Y_2O_3 ceramics is the simultaneous use of ZrO_2 and La_2O_3 aids [12-14], but the negative effects of them are also combined.

Another approach for the fabrication of Yb:Y_2O_3 laser ceramics is based on hot pressing of nanopowders or its combination with Hot Isostatic Pressing (HIPing). The mass transfer during the consolidation of green bodies under hot pressing is usually intensified by the use of liquid-phase sintering aids enhancing the ion diffusion. One example is lithium fluoride (LiF) which forms a liquid phase within the temperature range of 850-1200 °C and then almost completely evaporates from the sintered material. Moreover, LiF interacts with carbon-containing impurities and prevents them from entering the ceramics at the stage of open porosity. We are not aware of any data in the literature reporting on detrimental effects of LiF on the spectroscopic properties of sesquioxide ceramics. One should only mention a significant growth of the mean size of the grains when using liquid-phase sintering aids. This, together with the possible segregation of residual LiF at the grain boundaries may reduce the hardness of ceramics.

The idea to use LiF as a sintering aid during the synthesis of undoped Y_2O_3 ceramics was first proposed by Lefever *et al.* [16]. Since then, several studies focused on updating this

approach [16,17]; as for Yb:Y_2O_3 laser ceramics, there exist publications only from one group [3,18]. Sanghera *et al.* reported on a diode-pumped 2 at.% Yb:Y_2O_3 ceramic laser delivering 0.6 W at 1076 nm with a reasonably high slope efficiency of 44.6% [3]. However, almost no details about the synthesis of such ceramics were provided.

In the present work, we describe for the first time the results on the fabrication of Yb:Y_2O_3 laser ceramics by hot pressing of powders (obtained by the self-propagating high-temperature synthesis) with the use of LiF as a sintering aid. We also report on the spectroscopic properties and laser performance of such ceramics.

2. Synthesis of the ceramics

The nanopowders of ytterbium-doped yttrium oxide (Yb:Y_2O_3) were obtained by the self-propagating high-temperature synthesis (SHS) with the use of metal nitrates as oxidants and aminoacetic acid (glycine) as a fuel. The starting reagents were yttrium, Y_2O_3, and ytterbium, Yb_2O_3, oxides (purity: 99.99%, supplier: Lanhit, Russia), nitric acid HNO_3 (99.9999%), glycine NH_2CH_2COOH (99.9%) and lithium fluoride LiF (99.9%) (supplier: Khimreaktiv, Russia).

Water solutions of the metal nitrates were obtained by dissolving 9.7208 g of Y_2O_3 and 0.7882 of Yb_2O_3 in a stoichiometric amount of nitric acid upon heating. The glycine was added to the solution in a molar ratio of 1.2:1 with respect to the metal nitrates. 0.084 g of LiF was added to the solution which corresponded to 0.8 wt% of sintering aid in the synthesized Yb:Y_2O_3 powder. The resulting precursor solution was evaporated at a temperature of ~110 °C and then placed in a resistance furnace preheated to 300 °C in a quartz flask. The heating initiated exothermic reactions between nitrate groups and glycine, followed by a self-propagating high-temperature synthesis process over the entire volume of the precursor. After the end of the combustion, white Yb:Y_2O_3 – LiF nanopowder was obtained, softly agglomerated in the form of a foam. The powder was then calcined in air at 750 °C for 30 min.

The powder was compacted in a stainless-steel mold at a pressure of ~10 MPa. The compact was isolated using a graphite paper, placed in a graphite mold (Ø13 mm) and consolidated by hot pressing in vacuum at a maximum temperature of 1550 °C and an uniaxial pressure of 50 MPa using a home-made equipment. The heating was carried out by graphite heaters; the residual pressure in the chamber was 10 Pa. The hot-pressed ceramic was subjected to HIP treatment (for 8 h at 1200 °C, then for 4 h at 1400 °C and a pressure of 100 MPa).

The obtained ceramic disks (Ø13 mm) were ground on both sides to a thickness of 1-2 mm and polished with a diamond suspension.

3. Experimental

The sinterability of the Yb:Y_2O_3 – LiF nanopowder was studied by dilatometric analysis using a linear displacement transducer (resolution: 5 μm) embedded in a hot press at a heating rate of 10 °C/min to a temperature of 1600 °C in vacuum under loading of 50 MPa.

The specific surface area (S_{BET}) of the yttria nanopowder was measured by nitrogen adsorption according to the Brunauer–Emmett–Teller (BET) method using the Meta Sorbi-MS Meta equipment. The average diameter of the particles (d_{BET}) was calculated assuming their spherical shape according to the following equation: $d_{BET} = 6/(\rho \times S_{BET})$, where ρ is the theoretical density of the material calculated by the additive method from the densities of pure components.

The morphology of the powders was studied using a Carl Zeiss Auriga scanning electron microscope (SEM) at an accelerating beam voltage of 3 keV with a secondary electron detector. The morphology of the fractured surface of the ceramic was studied using a Carl Zeiss MERLIN SEM microscope. The grain size distribution was obtained by the direct counting method (for more than 100 grains) using the ImageJ software. We have applied the shape factor of 1.2. The X-ray diffraction analysis of nanopowders and ceramics was performed on a Shimadzu XRD-7000 diffractometer.

All the spectroscopic studies were performed at room temperature (RT, 20 °C). The transmission spectra were measured using a spectrophotometer (LOMO SF-2000) in the spectral range of 190–1100 nm. The infrared spectra of the ceramic were recorded using an SIMEX FT-801 FT-IR spectrometer. The spectrum of the Yb^{3+} luminescence was measured using an optical spectrum analyzer (Ando AQ6315-E) with a Ti:Sapphire laser tuned to 920 nm as an excitation source. The luminescence decay curves for the nanopowders and the powdered ceramic sample were measured using a ns optical parametric oscillator (Horizon, Continuum), a 1/4 m monochomator (Oriel 77200), an InGaAs detector and an 8 GHz digital oscilloscope (DSA70804B, Tektronix).

The Raman spectrum was measured using a confocal microscope (inVia, Renishaw) equipped with a ×50 objective (Leica) and an Ar^+ ion laser (488.0 nm).

4. Results and discussion

4.1. Yb:Y_2O_3 – LiF powders

The powders obtained by SHS were calcined in air at 750 °C for 30 min to completely oxidize any residual carbon-containing substances. The typical SEM images of Yb:Y_2O_3 and Yb:Y_2O_3 – LiF powders are shown in Fig. 1. During the SHS, the temperature of the powders exceeded the melting point of LiF (848 °C) for a few seconds. Nevertheless, there occurred a noticeable change of the morphology of the powders containing the sintering aid as compared to those without LiF. The latter promotes the mass transfer in powders and instead of a plate-shaped morphology (burst foam bubbles formed during SHS), they exhibit more equiaxed shape.

The bulk density of Yb:Y_2O_3 – LiF powders increased by a factor of ~1.5 as compared to that of Yb:Y_2O_3 ones, while the specific surface area decreased from 77 to 14 m^2/g, respectively. The corresponding average BET-equivalent particle diameters d_{BET} were 15 and 86 nm, respectively.

The XRD analysis of the Yb:Y_2O_3 powders did not reveal any other phases except that of the cubic yttrium oxide. However, for the Yb:Y_2O_3 – LiF powders, weak diffraction peaks at $2\theta = 27.7°$ and 32.4° are observed. Their assignment is complicated. Considering the

possible constituting chemical elements (Y, O, Yb, F), we suggest the presence of traces of $YbF_{2.37}$ and $Y_{17}O_{14}F_{23}$, respectively. The formation of oxyfluoride phases ($Dy_{1+x}O_{3x}F_{3-3x}$ and DyOF) in the LiF - rare earth oxide (Dy_2O_3) system was observed previously [19]. It also explains the absence of formation of lithium fluoride melt during sintering (see below). The effect of dopants (2% Yb and 1% LiF) on the lattice parameter was not significant: a = 10.604 ± 0.035 Å and 10.625 ± 0.032 Å for Yb:Y_2O_3 and Yb:Y_2O_3 – LiF powders, respectively, because within the measurement error, it coincided with the tabulated value for undoped yttrium oxide, a = 10.610 Å (JCPDS card No. 00-041-1105). However, LiF noticeably affected the powder crystallinity and the crystallite sizes. It can be seen from Fig. 2 that the diffraction peaks for the SHS Yb:Y_2O_3 – LiF powder are much more intense and narrower as compared to those for the Yb:Y_2O_3 one.

The introduction of LiF at the stage of the powder synthesis instead of the subsequent mixing by joint grinding or precipitation from a solution to the particle surface is more preferable for SHS powders. The rounded shape of the nanoparticles improves the density uniformity in the green bodies and ensures the degassing under hot pressing before forming closed porosity. The smaller specific surface area reduces the absorption of moisture, carbon dioxide and other impurities from air.

The shrinkage curve of the Yb:Y_2O_3 powder shown in Fig. 3 has the classical S-shape. The maximum shrinkage rate is observed at a temperature around 730 °C. Such a low sintering temperature is due to the small grain size, the flat shape of the particles, and the applied uniaxial pressure, which provides a closer contact of the particles. Without the use of external pressure, changes in morphology and sintering in SHS rare-earth oxide powders occur simultaneously. The poor contact between the particles results in a complex and heterogeneous shrinkage curve [20,21]. Despite the low initial sintering temperature of Yb:Y_2O_3, the shrinkage continues in a broad range of temperatures and the full densification is reached only at 1550-1600 °C.

The shrinkage curve of the Yb:Y_2O_3 – LiF powder also shown in Fig. 3 has a more complex form with three extremes observed with dependence of the shrinkage rate on the temperature. The first one at low temperature with a maximum around 300 °C is related to rearrangement and sliding of particles; the same behavior was observed during SPS of Y_2O_3 – LiF [17]. The next maximum of the shrinkage rate is probably associated with a change in the morphology of particles during heating, while the highest temperature one - with the beginning of the sintering aid (LiF) action. A similar explanation was given for the two high-temperature shrinkage peaks during sintering of Sc_2O_3 – LiF SHS powders [22]. However, it is noteworthy that both maxima appear at temperatures lower than the melting point of LiF. Thus, unlike, e.g., hot pressing of magnesium aluminate spinel with LiF addition [23], in our case the presence of liquid-phase sintering is not so obvious. There is a low-melting LiF-YF_3 eutectic with a LiF content of about 80 mol% and a melting point of less than 700 °C. But it is more likely that the action of lithium fluoride is limited to the creation of oxygen vacancies and activation of diffusion processes of mass transfer in yttrium oxide. The shrinkage of the Yb:Y_2O_3 – LiF compact almost completely finishes about 1400 °C. The lower shrinkage of the Yb:Y_2O_3 – LiF sample compared to that of the Yb:Y_2O_3 one is caused by its higher

green body density due to the better pressibility of the powder with more equiaxed shape and larger particle size.

4.2. Optical transmission of the ceramics

The hot pressing of the powders without the sintering aid leads to their consolidation as ceramics without reaching its full density. The in-line transmission at the wavelength of 1.1 μm does not exceed half from the theoretical value ($T_0 = 2n/(n^2 + 1) = 82.4\%$, this value accounts for multiple light reflections and calculated using the refractive index $n = 1.900$ [24]), see Fig. 4. This is due to light scattering at the residual pores and light absorption by carbon-containing impurities. The latter are probably formed because of the incomplete removal of adsorbed carbon dioxide from the atmosphere present during the synthesis, as well as possible reactions of disproportionality of carbon-containing gases formed from the graphite mold of the hot press: e.g., residual oxygen released because of the partial reduction of yttrium oxide can interact with graphite elements of the press forming carbon monoxide which disproportionates at the powder surface to carbon oxide (IV) and elementary carbon. Such ceramics are brown, see the inset in Fig. 4. Carbon in Yb:Y_2O_3 ceramic is also manifested by absorption at ~4.9 μm associated with carbon monoxide trapped in pores. After hot pressing, the ceramic fabricated from nanopowders containing the sintering aid looks gray, Fig. 4, while much less pronounced than in the above-described case. The in-line transmission of ceramics is also much higher in the visible, near- and mid-IR spectral ranges. The transmission range of this ceramic is 0.24 – 9.5 μm.

The most complicated aspect of hot pressing is the proper dynamics of removal of LiF. This is because this process strongly depends on multiple factors, such as the heating rate, the durations of isothermal holds, the moment and the rate of application of an uniaxial pressure, the pressure in the chamber, the composition of the residual atmosphere, the dispersity, the morphology of the powders, the content of LiF, etc. At the initial stage, LiF serves as a lubricant and allows the nanoparticles to slide with respect to each other which leads to filling large pores and a formation of an optimum compact microstructure for subsequent sintering. The LiF vapors react with carbon-containing impurities and promote their removal from the sample volume, as well as prevent their back-penetration. However, LiF should be almost completely removed at the stage of open porosity. The remaining sintering aid creates vapor pressure in closed pores and prevents their healing. Moreover, LiF may form secondary phases with Yb_2O_3 and Y_2O_3 which are neither removed even during a long high temperature hold under hot pressing nor under subsequent HIPing. Typically, the excess of LiF is revealed as a translucent spot at the center of the ceramic disk which is related to light scattering at the secondary phases and / or residual μm-range pores. From the other hand, a too early removal of LiF reduced the mass transfer rate and greatly grown particles are lacking the driving force for their final densification. This leads to a white (because of the pores) or black (because of the pores containing carbon) boundary of the ceramic disk. It is also possible that both types of defects are present (when there is an expense of LiF in the center and its lacking at the boundary), so that only a toroid-shaped part of the ceramic is remaining transparent.

The optimization of the conditions for hot pressing may help to reach the transmission of the ceramics close to its theoretical limit, as it was shown by Majima *et al*. for undoped Y_2O_3 [21]. However, a certain residual porosity was still present in samples being unfavorable for laser applications. In addition, this process is hardly reproducible. It is much easier to fabricate ceramic samples after hot pressing with a transmission exceeding 65-70% at ~1 μm. Under the conditions of uniform microstructure over the ceramic disk, the subsequent HIP treatment leads to ceramics of laser quality. For HIPing, the optimum conditions were determined as follows: first, a long hold (≥8 hours) at relatively low temperatures (1000-1200 °C) with a subsequent heating and another hold at 1400-1600 °C. Most probably, during the lower-temperature hold, the residual LiF is still removed, while the higher-temperature hold heals the nanopores. HIPing without the isothermal hold at 1000-1200 °C typically does not allow to reach high transmission about 80% at ~1.1 μm, and in certain cases, the transmission is even reduced as compared to samples obtained just by hot pressing.

4.3. Microstructure of ceramics

Figure 5 shows typical SEM images of the fractured surfaces of ceramic samples after hot pressing. The Yb:Y_2O_3 ceramic exhibits sub-μm grains and a noticeable number of pores with a size of ~500 nm or less in triple points, Fig. 5(a,c). Since the pores are comparable in size to the ceramic grains, they cannot be healed during HIPing. In contrast, for the Yb:Y_2O_3 – LiF ceramic, the grains are by order of magnitude larger due to the action of the sintering additive, and only a few pores can be found.

The morphology of the fractured surface of the ceramic fabricated from Yb:Y_2O_3 – LiF nanopowders was also studied after HIPing, see Fig. 6. The observed intragranular fracture indirectly indicates that there is almost no segregation of the sintering aid at the grain boundaries which may weaken them as compared to the grains themselves. For example, the fracture of Y_2O_3 [21] and Sc_2O_3 [20] ceramics fabricated with the use of LiF as a sintering aid but did not subjected to HIPing occurred at the grain boundaries.

The typical grain size distribution is shown at the inset of Fig. 6. The mean grain size is 55 μm. Probably due to the HIPing temperature not exceeding the hot pressing temperature, no noticeable increase in the average grain size is observed.

The XRD powder analysis of the ceramics fabricated from the Yb:Y_2O_3 and Yb:Y_2O_3 – LiF nanopowders did not reveal any structure differences nor peculiarities of their composition, Fig. 7. A single cubic phase of yttrium oxide was detected (sp. gr. $Ia\bar{3}$ - T^7_h, No. 206). The corresponding lattice parameters are a = 10.602 ± 0.025 Å and a = 10.604 ± 0.014 Å for Yb:Y_2O_3 and Yb:Y_2O_3 – LiF ceramics, respectively. Within the measurement error, they coincide with the tabulated value for undoped Y_2O_3. In the XRD patterns of both ceramics, very weak diffraction peaks at 2θ = 26.3° and 30.1° most likely indicate the reduced (metallic) ytterbium on the surface due to a direct contact with carbon. The gray tint of ceramics is probably related to this.

In the cubic (bixbyite or C-type) structure of sesquioxides including Y_2O_3, there exist two crystallographic sites for rare-earth ions (Y^{3+}) with local symmetries C_2 and C_{3i} and VI-

fold oxygen coordination. The ratio of the C_2 to C_{3i} sites is 3:1. The Yb^{3+} dopant ions replace for the host-forming Y^{3+} cations in both sites. The optical properties of C-type sesquioxides are mostly determined by the majority of rare-earth ions (approximately 3/4) residing in the C_2 sites. This is because for the C_{3i} sites, the electric-dipole transitions are forbidden due to the inversion symmetry. Due to the closeness of ionic radii of Y^{3+} (0.90 Å) and Yb^{3+} (0.868 Å) [25], weak lattice distortion is expected upon doping.

4.4. Optical spectroscopy

The absorption spectrum of the Yb:Y_2O_3 ceramic at 850-1150 nm is shown in Fig. 8. The absorption is due to the $^2F_{7/2} \rightarrow {}^2F_{5/2}$ transition of Yb^{3+} ions. The absorption cross-sections were calculated from the measured absorption coefficient: $\sigma_{abs} = \alpha_{abs}/N_{Yb}$, where $N_{Yb} = 5.31\times10^{20}$ cm^{-3} is the total Yb^{3+} ion density.

The maximum σ_{abs} is 1.99×10^{-20} cm^2 at 976.5 nm and the corresponding absorption bandwidth (full width at half maximum, FWHM) is only 1.2 nm. It corresponds to the so-called zero-phonon line (ZPL) transition of Yb^{3+} ions (the transition between the lower-lying Stark sub-levels of the two multiplets). At shorter wavelengths, there is another weaker peak centered at 950.6 nm with much broader FWHM of 10 nm which appears more attractive for pumping by InGaAs diode lasers due to weaker sensitivity to the temperature drift of the diode wavelength.

The stimulated-emission (SE) cross-sections, σ_{SE}, for the $^2F_{5/2} \rightarrow {}^2F_{7/2}$ transition of Yb^{3+} ions were derived by two methods. The first one is the Füchtbauer–Ladenburg (F-L) equation [26]:

$$\sigma_{SE}(\lambda) = \frac{\lambda^5}{8\pi < n >^2 \tau_{rad} c} \frac{W'(\lambda)}{\int \lambda W'(\lambda) \mathrm{d}\lambda}, \quad (1)$$

where, λ is the light wavelength, $<n> = 1.90$ is the refractive index of the ceramic at ~1 μm [24], $\tau_{rad} = 0.89$ ms is the radiative lifetime of the emitting state ($^2F_{5/2}$), c is the speed of light and $W'(\lambda)$ is the luminescence spectrum corrected for the spectral response of the set-up.

The second one is the reciprocity method (RM) [27]:

$$\sigma_{SE}(\lambda) = \sigma_{abs}(\lambda) \frac{Z_1}{Z_2} \exp\left(-\frac{hc/\lambda - E_{ZPL}}{kT} \right), \quad (2)$$

where h is the Planck constant, k is the Boltzmann constant, T is the temperature (RT), E_{ZPL} is energy corresponding to the ZPL transition, and Z_m are the partition functions of the lower ($m = 1$, $^2F_{7/2}$) and upper ($m = 2$, $^2F_{5/2}$) multiplets. The previously reported crystal-field splitting for Yb^{3+} ions in C_2 sites in Y_2O_3 was used: $^2F_{7/2}$ = (0, 320, 528 and 930 cm^{-1}) and $^2F_{5/2}$ = (10242, 10518 and 11028 cm^{-1}) [28]. This lead to the following partition functions: $Z_1 = 1.292$ and $Z_2 = 1.278$, respectively, so that $Z_1/Z_2 = 1.011$.

The results on σ_{SE} calculated by the two methods are shown in Fig. 8. They are in good agreement (considering the effect of reabsorption on the measured luminescence spectrum) indicating the correctness of the selected τ_{rad} value. The maximum σ_{SE} is 2.01×10^{-20} cm^2 at 976.5 nm (ZPL). As Yb^{3+} ions represent a quasi-three-level laser scheme with reabsorption, the laser operation is expected at the wavelengths being longer than the ZPL. In this spectral

range, σ_{SE} reaches 0.90×10^{-20} cm^2 at 1030.4 nm (F-L equation) and the corresponding emission bandwidth (FWHM) is 14 nm.

The estimated radiative lifetime agrees with the previous studies for Yb:Y_2O_3 [29,30].

The luminescence decay curve for the Yb:Y_2O_3 ceramic fabricated using LiF sintering aid is shown in Fig. 9. Prior to the measurement, the sample was powdered to avoid the effect of radiation trapping on the lifetime. The decay time, obtained via a single-exponential fit, amounts to τ_{lum} = 0.797 ms. In Fig. 9, the decay curves for Yb:Y_2O_3 and Yb:Yb_2O_3 – LiF powders are also shown. Both of them are not single-exponential; the mean decay times, $<\tau_{lum}>$, are drastically different, 0.175 ms and 0.908 ms, respectively, indicating a strong luminescence quenching in the powder without LiF. This highlights the importance of LiF for achieving good spectroscopic properties of the ceramic.

The Raman spectrum of the Yb:Y_2O_3 ceramic fabricated using LiF sintering aid is shown in Fig. 10. For C-type sesquioxides, at the center of the Brillouin zone, the set of irreducible representations is $\Gamma = 4A_g + 4E_g + 14F_g + 5A_{2u} + 5E_u + 16F_u$, among which the A_g, E_g, and F_g modes are Raman-active, F_u is IR active and A_{2u} and E_u are silent [31,32]. The number of the observed modes for the ceramic (12) is less than the theoretical one (22). The most intense band is centered at 375 cm^{-1} (FWHM = 11.5 cm^{-1}) and assigned to a combination of a A_g and F_g modes (related to stretching vibrations). In the small-frequency range, there are three distinct bands characteristic of the C-type sesquioxide structure, centered at 127, 160 and 192 cm^{-1} and related to the F_g, $A_g + F_g$ and $E_g + F_g$ modes, respectively. The maximum phonon frequency is 591 cm^{-1}.

Raman spectroscopy was previously suggested as a method for detecting elementary carbon impurities in transparent ceramics [33,34]. The inspection of the Raman spectrum of the Yb:Y_2O_3 - LiF ceramic in the range of 1000 - 2000 cm^{-1} did not reveal any characteristic bands of C indicating a weak presence of such impurities.

4.5. Laser set-up

The laser set-up is schematically shown in Fig. 11. The laser element was a 2 at.% Yb:Y_2O_3 ceramic fabricated using the LiF sintering aid and having a thickness of 1.62 mm was polished to laser-grade quality and left uncoated. The measured in-line transmission for this ceramic sample at ~1.1 μm was T = 78.3%. It was mounted on a passively cooled Cu-holder using a silver paint to improve the thermal contact. The linear laser cavity was made up of a flat pump mirror (PM) coated for high transmission (HT, T > 97%) at 0.88-0.99 μm and for high reflection (HR, R > 99.9%) at 1.02-1.20 μm, and a set of concave output couplers (OCs) with a radius of curvature (RoC) of -100 mm and a transmission T_{OC} in the range of 1% - 20% at 1.0-1.1 μm. The geometrical cavity length was ~100 mm (a hemispherical cavity). The laser element was placed near the PM with a small separation less than 1 mm. For comparison, we have also used flat OCs with the same coatings. In that case, both the PM and the OC were placed as close as possible to the ceramic element resulting in a quasi-microchip design (cavity length: ~1.7 mm).

As a pump source, we used a CW Ti:Sapphire laser (model 3900S, Spectra Physics) delivering up to ~3 W at 976.4 nm in the fundamental mode ($M^2 \approx 1$). The pump wavelength

corresponded to the ZPL line of Yb^{3+} ions, Fig. 8. The pump was focused into the ceramic element through the PM using a plano-convex uncoated CaF_2 lens (f = 100 mm) resulting in a measured pump spot radius w_P of 60±10 μm. All the used OCs provided high reflectance at the pump wavelength (R > 90%), so that the pumping was in double-pass. The total pump absorption under lasing conditions was determined from pump-transmission measurement at the threshold pump power (for each OC) accounting for the Fresnel losses at the uncoated ceramic element and the double-pass of the pump. It decreased with the output coupling, i.e., from 69.1% (T_{OC} = 1%) down to 53.3% (T_{OC} = 20%), representing the effect of absorption saturation (ground-state bleaching). The residual (non-absorbed) pump radiation was blocked by a long-pass filter (FEL1000, Thorlabs). To measure the spectra of the laser emission, we used an optical spectrum analyzer (Ando AQ6315-E). The beam profile in the far-field was measured using a CCD camera.

4.6. Laser performance

First, the laser experiments were performed for the hemispherical cavity design. The Yb:Y_2O_3 ceramic laser generated a maximum output power of 383 mW at 1028-1031 with a slope efficiency η of 28.7% (with respect to the absorbed pump power P_{abs}) and a laser threshold P_{th} of 0.29 W (for 10% output coupler), Fig. 12(a). The input-output dependence was nonlinear near the laser threshold and its fitting was performed for pump powers well exceeding P_{th}. With increasing the output coupling, the laser threshold gradually increased, from 0.15 W (T_{OC} = 1%) to 0.36 W (T_{OC} = 20%). The typical spectra of the laser emission are shown in Fig. 12(b); the laser emission was unpolarized. The spectra were weakly dependent on the output coupling and the laser emission occurred around 1.03 μm corresponding to a local maximum in the gain spectra for high inversion ratios.

A better performance was achieved by implementing the quasi-microchip cavity design, Fig. 12(a). Using T_{OC} = 10%, the laser generated 735 mW at 1027-1034 nm with η = 64.5% and a laser threshold of 0.28 W. At the maximum available incident pump power of 2.81 W, the optical-to-optical efficiency of the laser η_{opt} amounted to 26.2%. Further power scaling was limited by the available pump. No thermal roll-over nor fracture of the ceramic were observed. The emission spectrum of the ceramic laser in the quasi-microchip geometry was broadened as compared to that for the hemispherical cavity, Fig. 12(b). Its multiple line structure is due to the etalon (Fabry-Perot) effects at the ceramic / mirror interfaces. The laser operated in the fundamental transverse mode and the mode profile in the far-field was nearly-spherical, see the inset in Fig. 12(a). The improved laser performance for the quasi-microchip cavity is assigned to better matching between the pump and laser modes, as well as lower passive losses in the compact cavity.

The use of a simple model of a quasi-three-level laser [35] yielded a round-trip passive loss L of ~5% which corresponds to the coefficient of passive losses in the ceramic δ_{loss} of about 0.15 cm^{-1}.

The laser excitation curve for the Yb:Y_2O_3 ceramic, i.e., the plot of the output power vs. the pump wavelength at a fixed incident pump power (P_{inc} = 1.77 W), was measured to confirm the selection of λ_P, Fig. 13. The measured curve well followed the absorption cross-

section spectrum with a maximum at 976.4 nm (pumping into ZPL of Yb^{3+} ions). Another less intense while broader peak was observed at ~950 nm (however, stronger heat loading is expected when using this pump wavelength). It was possible to achieve laser operation for λ_P in the range of 899- 985 nm.

The only previous result on the laser performance of Yb:Y_2O_3 ceramic fabricated using the LiF sintering additive was reported by Sanghera *et al.* [3]: under diode-pumping at 940 nm, the ceramic laser generated 0.6 W at 1076 nm with η = 44.6% (vs. the absorbed pump power). In the present work, we report on the better performance (for the quasi-microchip laser geometry) which is ascribed to good optical quality of the ceramic, good mode-matching and longer pump wavelength leading to higher Stokes efficiency.

5. Conclusions

Laser-quality Yb:Y_2O_3 ceramic has been successfully produced by a combination of hot pressing (HPing) at 1550 °C / 50 MPa followed by a two-stage Hot Isostatic Pressing (HIPing) at 1200 - 1400 °C / 100 MPa, using nanopowders obtained by self-propagating high-temperature synthesis (SHS). Lithium fluoride sintering aid was added to the SHS precursor, which allowed it to be uniformly distributed in the powder, resulting in a ~1.5 times increase in the bulk density, a reduction in the specific surface area from 77 to 14 m^2/g and a change in morphology from plate-shaped to more equiaxed. The maximum shrinkage rate of the compacted Yb:Y_2O_3 – LiF powders was observed at ~800 °C, which is lower than the melting temperature of the sintering aid. Despite the absence of a liquid phase during HPing, LiF stimulates sintering of powders, as well as drastically reduces the carbon contamination of ceramics. Subsequent HIPing of the Yb:Y_2O_3 – LiF ceramics at relatively low temperatures (1000-1200 °C) with a long hold (≥8 hours) probably gets rid of the remaining sintering aid, and another higher-temperature hold at 1400-1600 °C heals the nanopores. The resulting ceramic has a dense structure with an average grain size of 55 μm. The good optical quality of ceramics was confirmed by laser experiments. A continuous-wave 2 at.% Yb:Y_2O_3 ceramic micro-laser generated an output power of 735 mW at 1027-1034 nm with a slope efficiency as high as 64.5% and a laser threshold of 0.28 W.

Acknowledgements

The work at IChHPS was performed within the state assignment No. 0095-2019-005.

References

1. J. Lu, K. Takaichi, T. Uematsu, A. Shirakawa, M. Musha, K. Ueda, H. Yagi, T. Yanagitani, A.A. Kaminskii, Yb^{3+}:Y_2O_3 ceramics - a novel solid-state laser material, Jpn. J. Appl. Phys. 41 (2002) L1373–L1375.

2. S.S. Balabanov, Y.V. Bykov, S.V. Egorov, A.G. Eremeev, E.M. Gavrishchuk, E.A. Khazanov, I.B. Mukhin, O.V. Palashov, D.A. Permin, V.V. Zelenogorsky, Transparent Yb:$(YLa)_2O_3$ ceramics produced by self-propagating high-temperature synthesis and microwave sintering, Opt. Mater. 35 (2013) 727–730.

3. J. Sanghera, S. Bayya, G. Villalobos, W. Kim, J. Frantz, B. Shaw, B. Sadowski, R. Miklos, C.

Baker, M. Hunt, I. Aggarwal, F. Kung, D. Reicher, S. Peplinski, A. Ogloza, P. Langston, C. Lamar, P. Varmette, M. Dubinskiy, L. Desandre, Transparent ceramics for high-energy laser systems, Opt. Mater. 33 (2011) 511–518.
4. H. Mingsheng, L. Jianbao, L. Hong, G. Gangfeng, L. Long, Fabrication of transparent polycrystalline yttria ceramics by combination of SPS and HIP, J. Rare Earths. 24 (2006) 222–224.
5. I.L. Snetkov, I.B. Mukhin, S.S. Balabanov, D.A. Permin, O. V Palashov, Efficient lasing in Yb:$(YLa)_2O_3$ ceramics, Quantum Electron. 45 (2015) 95–97.
6. V.V. Osipov, V.A. Shitov, R.N. Maksimov, V.I. Solomonov, Properties of transparent Re^{3+}:Y_2O_3 ceramics doped with tetravalent additives, Opt. Mater. 50 (2015) 65–70.
7. R.P. Yavetskiy, A.E. Balabanov, S. V. Parkhomenko, O.S. Kryzhanovska, A.G. Doroshenko, P. V. Mateychenko, A. V. Tolmachev, J. Li, N. Jiang, L. Gheorghe, M. Enculescu, Effect of starting materials and sintering temperature on microstructure and optical properties of Y_2O_3:Yb^{3+} 5 at% transparent ceramics, J. Adv. Ceram. 10 (2021) 49-61.
8. J. Wang, D. Yin, J. Ma, P. Liu, Y. Wang, Z. Dong, L.B. Kong, D. Tang, Pump laser induced photodarkening in ZrO_2-doped Yb:Y_2O_3 laser ceramics, J. Eur. Ceram. Soc. 39 (2019) 635–640.
9. S. Li, X. Zhu, J. Li, R. Yavetskiy, M. Ivanov, B. Liu, W. Liu, Y. Pan, Fabrication of 5 at.%Yb:$(La_{0.1}Y_{0.9})_2O_3$ transparent ceramics by chemical precipitation and vacuum sintering, Opt. Mater. 71 (2017) 56–61.
10. O.S. Kryzhanovska, V.N. Baumer, S.V. Parkhomenko, A.G. Doroshenko, R.P. Yavetskiy, A.E. Balabanov, A.V. Tolmachev, S.N. Skorik, J. Li, A. Kuncser, Formation peculiarities and optical properties of highly-doped $(Y_{0.86}La_{0.09}Yb_{0.05})_2O_3$ transparent ceramics, Ceram. Int. 45 (2019) 16002–16007.
11. S.S. Balabanov, Y. V Bykov, S. V Egorov, A.G. Eremeev, E.M. Gavrishchuk, E.A. Khazanov, I.B. Mukhin, O. V Palashov, D.A. Permin, V. V Zelenogorskii, Yb:$(YLa)_2O_3$ laser ceramics produced by microwave sintering, Quantum Electron. 43 (2013) 396–400.
12. G. Stanciu, F. Voicu, C.-A. Brandus, C.-E. Tihon, S. Hau, C. Gheorghe, G. Croitoru, L. Gheorghe, M. Dumitru, Enhancement of the laser emission efficiency of Yb:Y_2O_3 ceramics via multi-step sintering method fabrication, Opt. Mater. 109 (2020) 110411.
13. G. Stanciu, L. Gheorghe, F. Voicu, S. Hau, C. Gheorghe, G. Croitoru, M. Enculescu, R.P. Yavetskiy, Highly transparent Yb:Y_2O_3 ceramics obtained by solid-state reaction and combined sintering procedures, Ceram. Int. 45 (2019) 3217–3222.
14. I.L. Snetkov, V.V. Balashov, Thermo-optical properties of Ho:Y_2O_3 ceramics, Opt. Mater. 100 (2020) 109617.
15. R.A. Lefever, J. Matsko, Transparent yttrium oxide ceramics, Mater. Res. Bull. 2 (1967) 865–869.
16. K. Majima, N. Niimi, M. Watanabe, S. Katsuyama, H. Nagai, Effect of LiF addition on the preparation of transparent Y_2O_3 by the vacuum hot pressing method, J. Alloys Compd. 193 (1993) 280–282.
17. R. Marder, R. Chaim, G. Chevallier, C. Estournès, Effect of 1wt% LiF additive on the densification of nanocrystalline Y_2O_3 ceramics by spark plasma sintering, J. Eur. Ceram. Soc. 31 (2011) 1057–1066.
18. W. Kim, G. Villalobos, C. Baker, J. Frantz, B. Shaw, S. Bayya, B. Sadowski, M. Hunt, I. Aggarwal, J. Sanghera, Ceramic windows and gain media for high-energy lasers, Opt. Eng. 52

(2012) 021003-1-8.
19. C. Liao, S. Chen, X. Wang, B. Cai, J. Lin, Y. Jiao, Y. Zeng, Identification of ions present in LiF-DyF_3 melts and the mechanism of Dy_2O_3 dissolution therein, J. Rare Earths. 37 (2019) 211–217.
20. S. Balabanov, S. Filofeev, M. Ivanov, A. Kaigorodov, D. Kuznetsov, D.J. Hu, J. Li, O. Palashov, D. Permin, E. Rostokina, I. Snetkov, Fabrication and characterizations of holmium oxide based magneto-optical ceramics, Opt. Mater. 101 (2020) 109741-1-6.
21. S.S. Balabanov, D.A. Permin, E.Y. Rostokina, S. V. Egorov, A.A. Sorokin, D.D. Kuznetsov, Synthesis and structural characterization of ultrafine terbium oxide powders, Ceram. Int. 43 (2017) 16569–16574.
22. D.A. Permin, S.S. Balabanov, I.L. Snetkov, O.V. Palashov, A.V. Novikova, O.N. Klyusik, I.V. Ladenkov, Hot pressing of Yb:Sc_2O_3 laser ceramics with LiF sintering aid, Opt. Mater. 100 (2020) 109701-1-6.
23. S.S. Balabanov, A. V. Belyaev, A. V. Novikova, D.A. Permin, E.Y. Rostokina, R.P. Yavetskiy, Densification peculiarities of transparent $MgAl_2O_4$ ceramics—Effect of LiF sintering additive, Inorg. Mater. 54 (2018) 1045–1050.
24. Y. Nigara, Measurement of the optical constants of yttrium oxide, Jpn. J. Appl. Phys. 7 (1968) 404–408.
25. R.D. Shannon, Revised effective ionic radii and systematic studies of interatomic distances in halides and chalcogenides, Acta Crystallogr. Sect. A. 32 (1976) 751–767.
26. B. Aull, H. Jenssen, Vibronic interactions in Nd:YAG resulting in nonreciprocity of absorption and stimulated emission cross sections, IEEE J. Quantum Electron. 18 (1982) 925–930.
27. S.A. Payne, L.L. Chase, L.K. Smith, W.L. Kway, W.F. Krupke, Infrared cross-section measurements for crystals doped with Er^{3+}, Tm^{3+}, and Ho^{3+}, IEEE J. Quantum Electron. 28 (1992) 2619–2630.
28. A. Lupei, V. Lupei, S. Hau, Vibronics in optical spectra of Yb^{3+} and Ce^{3+} in YAG and Y_2O_3 ceramics, Opt. Mater. 63 (2017) 143–152.
29. L.D. Merkle, G. Alex Newburgh, N. Ter-Gabrielyan, A. Michael, M. Dubinskii, Temperature-dependent lasing and spectroscopy of Yb:Y_2O_3 and Yb:Sc_2O_3, Opt. Commun. 281 (2008) 5855–5861.
30. L. Zhang, W. Pan, J. Feng, Dependence of spectroscopic and thermal properties on concentration and temperature for Yb:Y_2O_3 transparent ceramics, J. Eur. Ceram. Soc. 35 (2015) 2547–2554.
31. N.D. Todorov, M. V. Abrashev, V. Marinova, M. Kadiyski, L. Dimowa, E. Faulques, Raman spectroscopy and lattice dynamical calculations of Sc_2O_3 single crystals, Phys. Rev. B. 87 (2013) 104301-1-5.
32. A. Ubaldini, M.M. Carnasciali, Raman characterisation of powder of cubic RE_2O_3 (RE=Nd, Gd, Dy, Tm, and Lu), Sc_2O_3 and Y_2O_3, J. Alloys Compd. 454 (2008) 374–378.
33. A. Goldstein, M. Katz, R. Boulesteix, A.I. Shames, C. Coureau, J. Raethel, X. Mateos-Ferre, P. Loiko, Sources of parasitic features in the visible range of oxide transparent ceramics absorption spectra, J. Amer. Ceram. Soc. 103 (2020) 4803-4821.
34. K. Morita, B.N. Kim, H. Yoshida, K. Hiraga, Y. Sakka, Distribution of carbon contamination in $MgAl_2O_4$ spinel occurring during spark-plasma-sintering (SPS) processing: I–effect of heating

rate and post-annealing, J. Eur. Ceram. Soc. 38 (2018) 2588-2595.
35. J.M. Serres, V. Jambunathan, P. Loiko, X. Mateos, H. Yu, H. Zhang, J. Liu, A. Lucianetti, T. Mocek, K. Yumashev, U. Griebner, V. Petrov, M. Aguiló, F. Díaz, Microchip laser operation of Yb-doped gallium garnets, Opt. Mater. Express. 6 (2016) 46-57.

List of figure captions

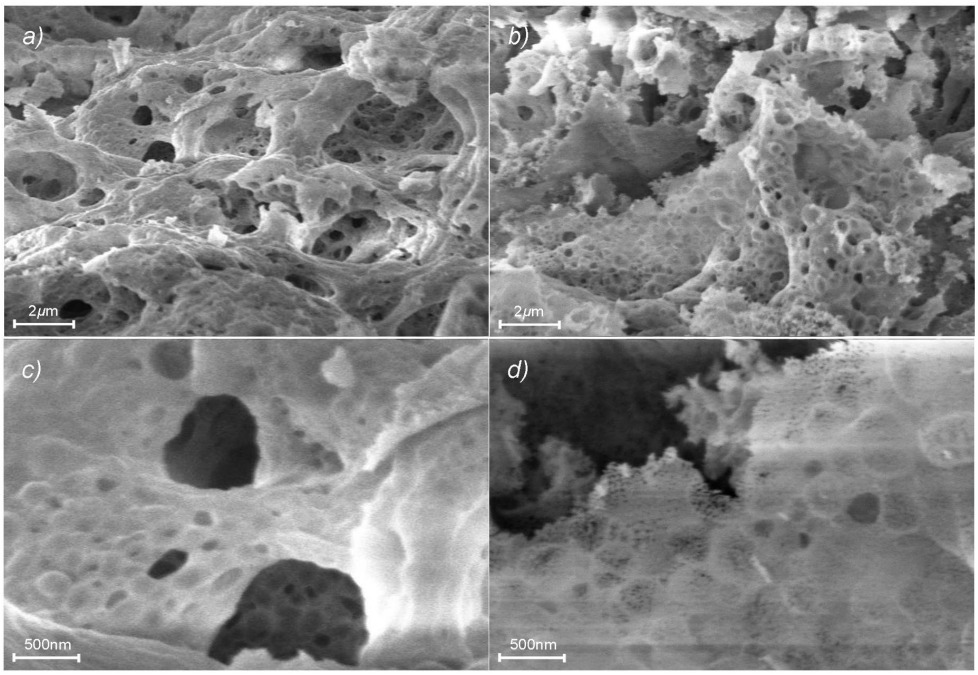

Figure 1. SEM images of (a,c) Yb:Y_2O_3 and (b,d) Yb:Y_2O_3 – LiF nanopowders obtained by self-propagating high-temperature synthesis.

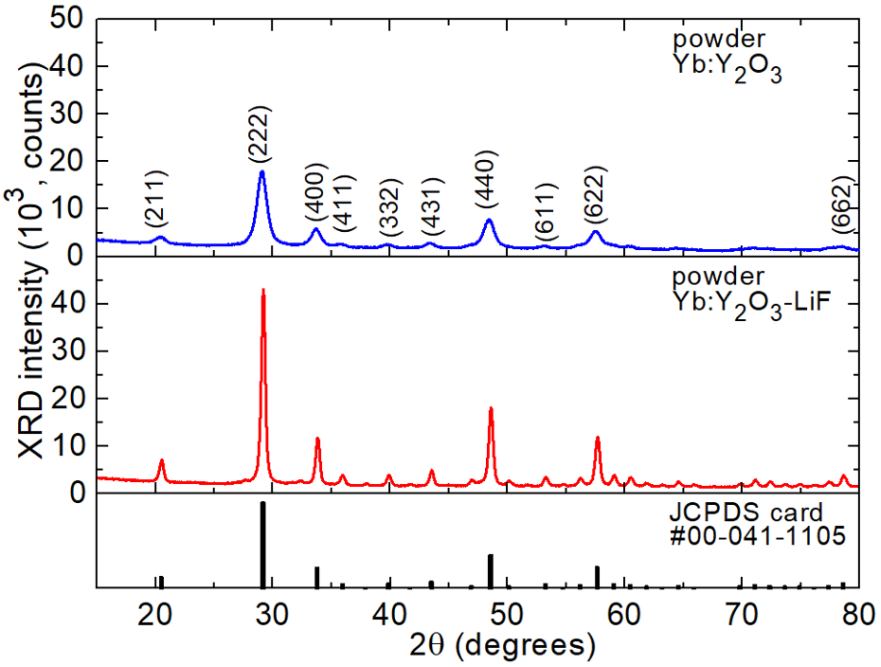

Figure 2. XRD patterns of Yb:Y_2O_3 and Yb:Y_2O_3 – LiF nanopowders obtained by self-propagating high-temperature synthesis. *Vertical dashes* – theoretical reflections for Y_2O_3 (JCPDS card #00-041-1105). Numbers denote the Miller's indices, (*hkl*).

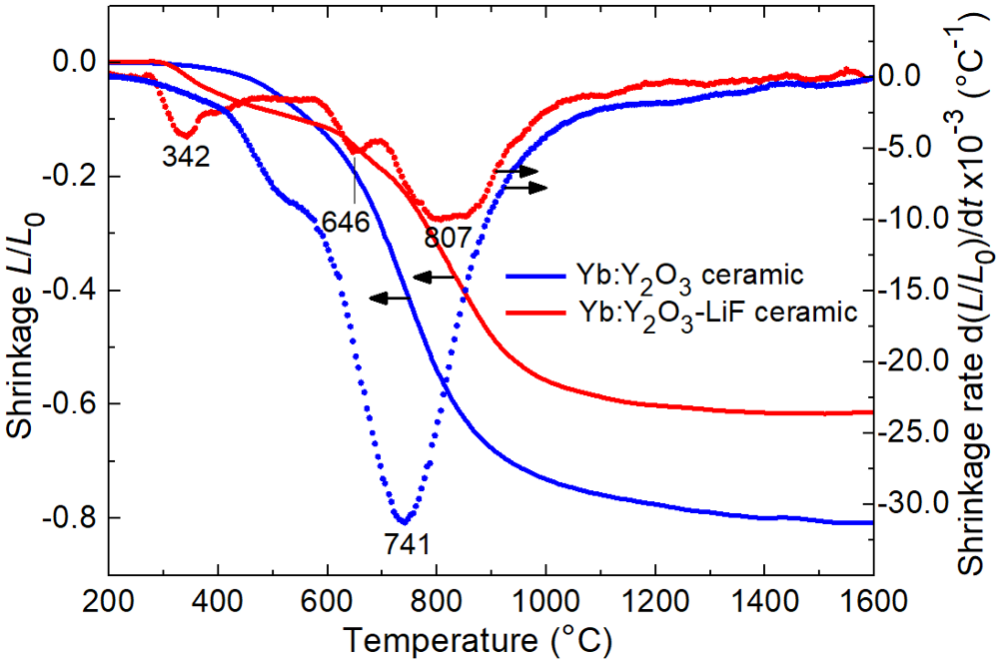

Figure 3. Shrinkage curves (*solid*) and shrinkage rate (*symbols*) of Yb:Y_2O_3 and Yb:Y_2O_3 – LiF green bodies.

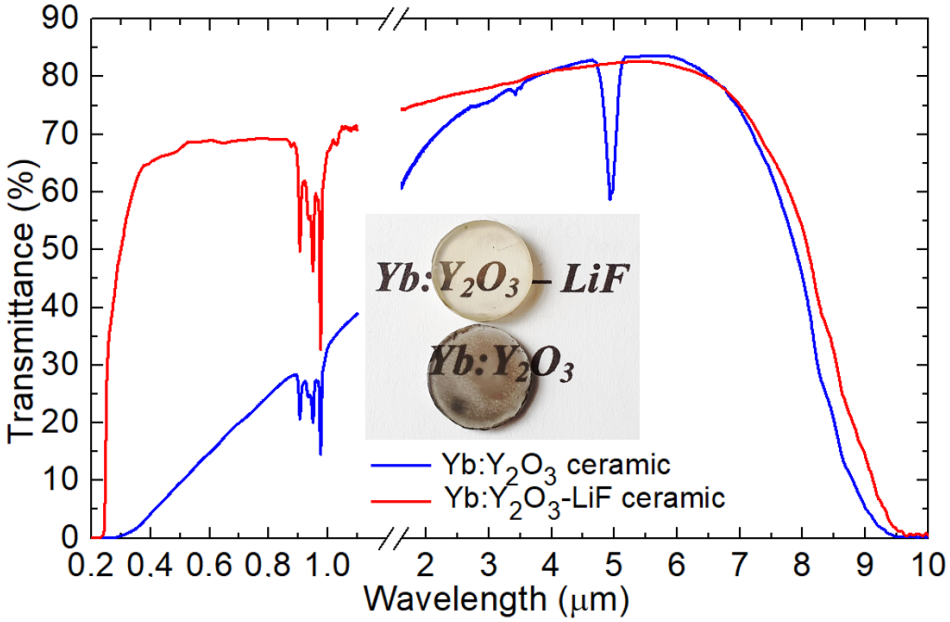

Figure 4. Transmission spectra of hot-pressed ceramics fabricated from Yb:Y_2O_3 and Yb:Y_2O_3 – LiF nanopowders, *inset* – photographs of the as-sintered and polished ceramic disks.

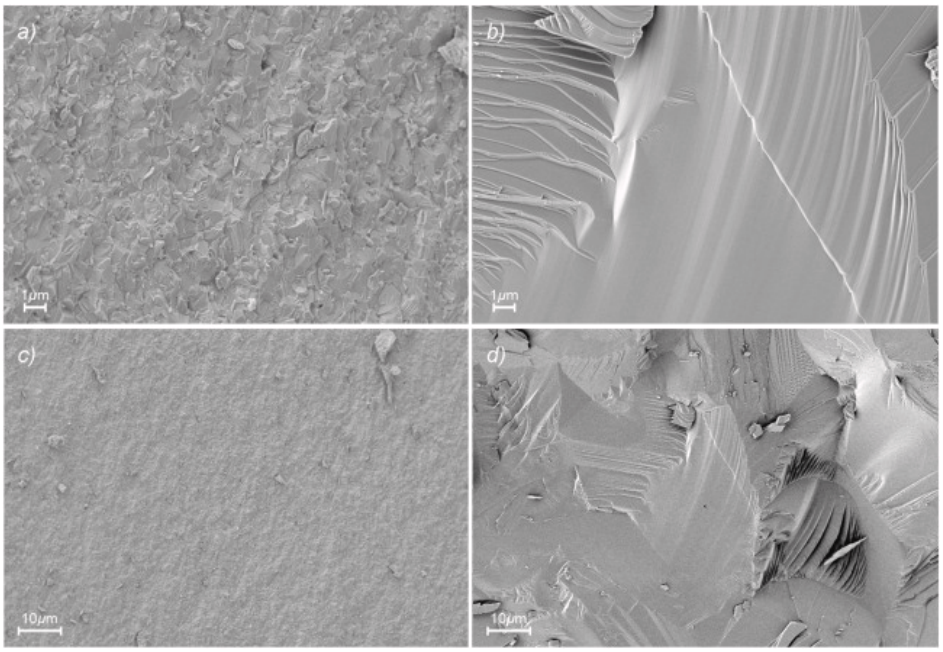

Figure 5. SEM images of the fractured surfaces of hot-pressed ceramics fabricated from (a,c) Yb:Y_2O_3 and (b,d) Yb:Y_2O_3 – LiF nanopowders.

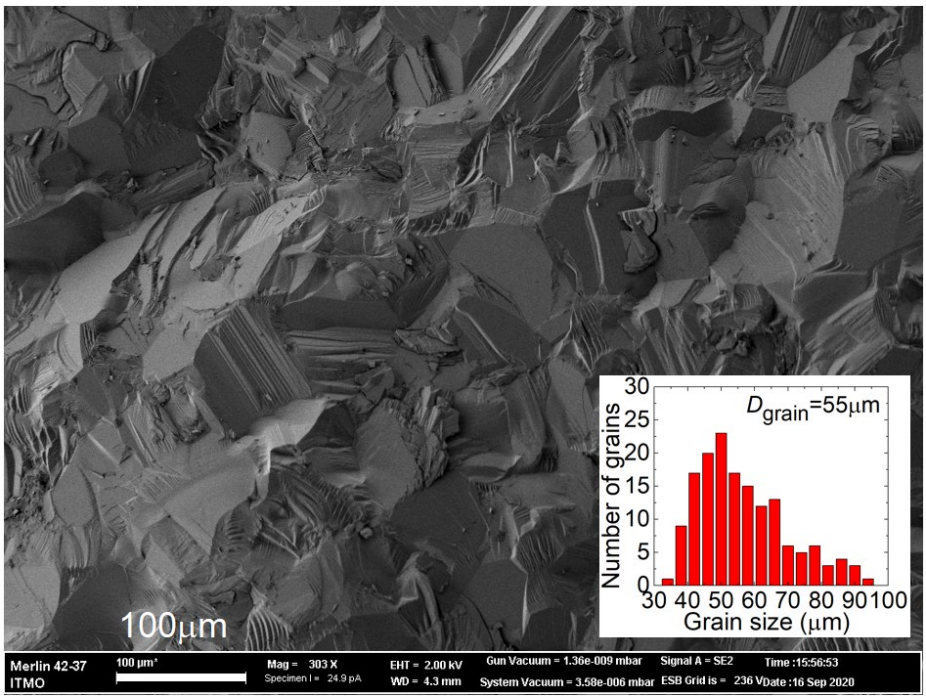

Figure 6. SEM image of the fractured surface of Yb:Y_2O_3 ceramic fabricated from Yb:Y_2O_3 – LiF nanopowders, after HIPing, *inset* – typical grain size distribution.

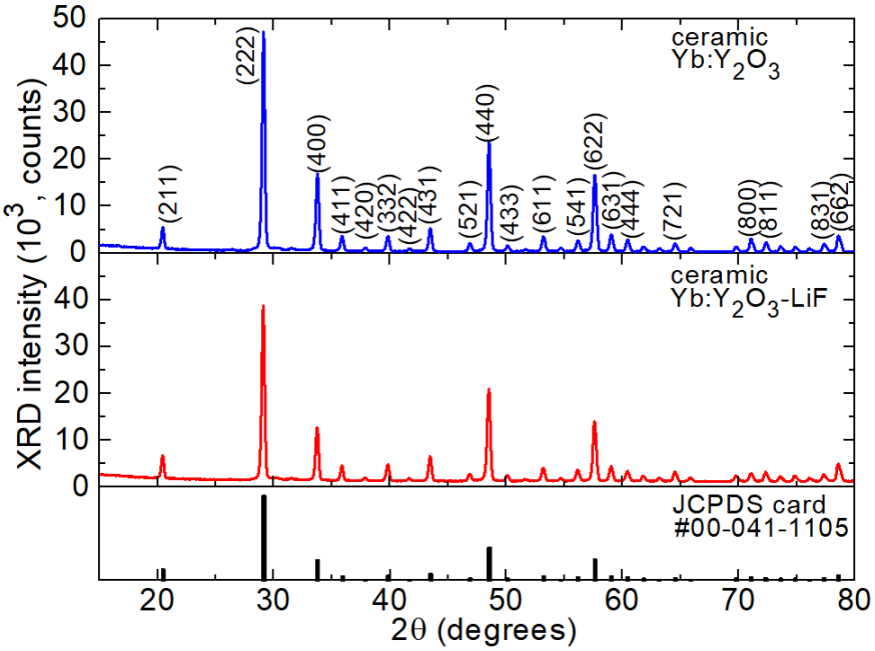

Figure 7. X-ray powder diffraction patterns of 2 at.% Yb:Y_2O_3 ceramics prepared from Yb:Y_2O_3 and Yb:Y_2O_3 – LiF nanopowders.

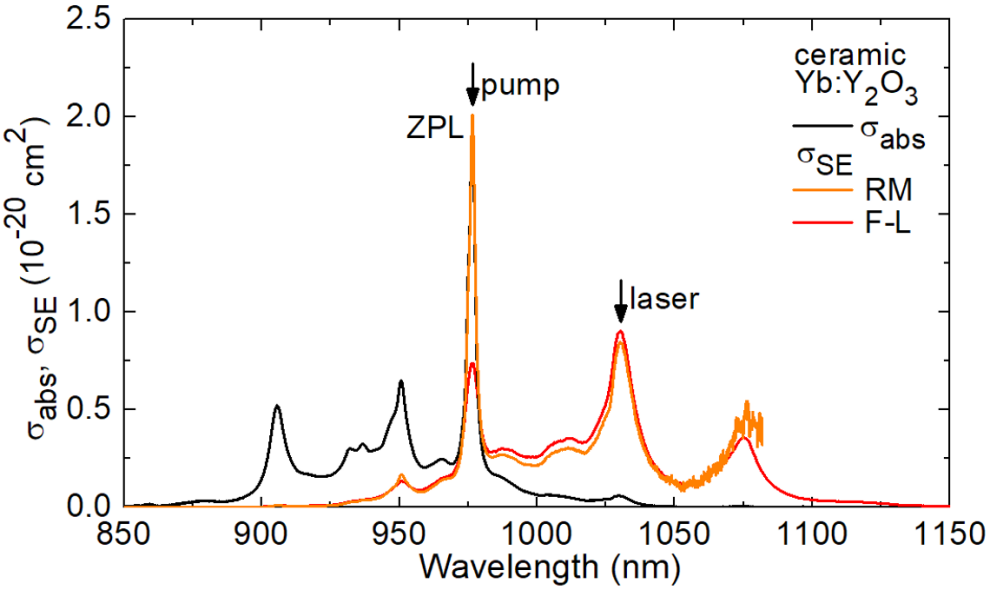

Figure 8. Absorption, σ_{abs}, and stimulated-emission (SE), σ_{SE}, cross-sections for the $^2F_{7/2} \leftrightarrow {}^2F_{5/2}$ transition of Yb^{3+} ions in the 2 at.% Yb:Y_2O_3 ceramics fabricated using LiF sintering additive. *Arrows* indicate the pump and laser wavelengths.

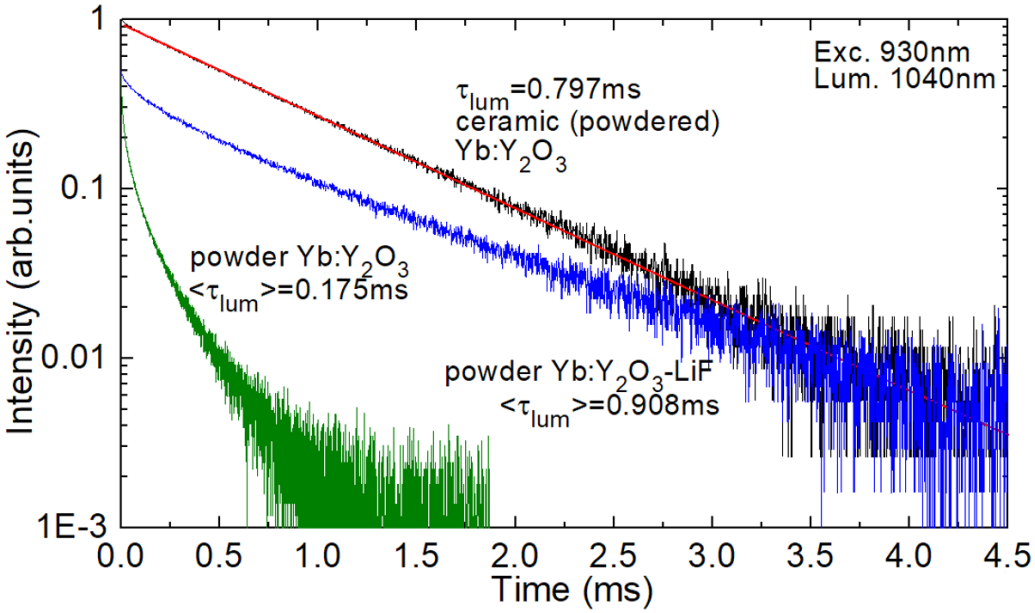

Figure 9. RT luminescence decay curves for Yb^{3+} ions in the Y_2O_3 ceramic fabricated using LiF sintering additive (powdered sample), Y_2O_3 and Y_2O_3 – LiF nanopowders, λ_{exc} = 930 nm, λ_{lum} = 1040 nm, τ_{lum} – decay time.

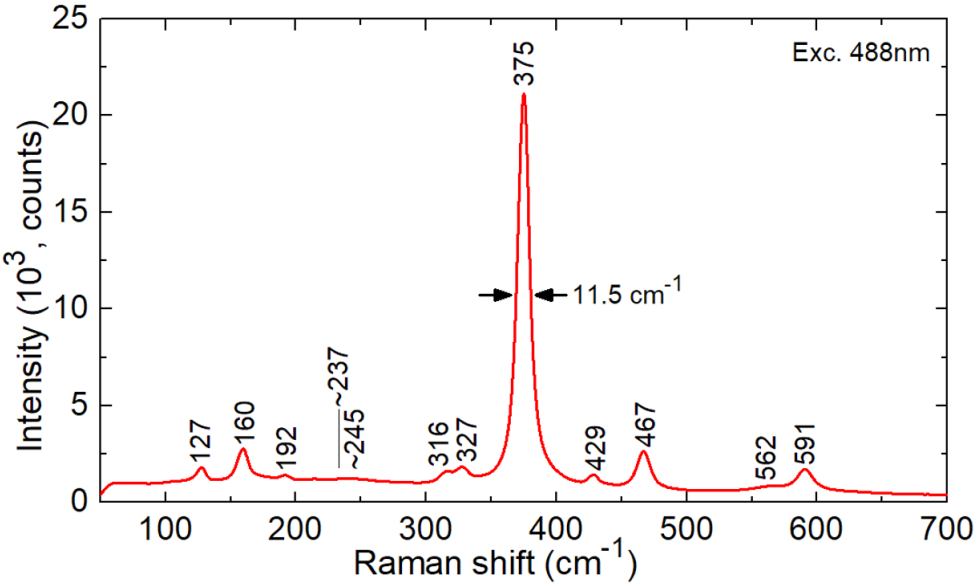

Figure 10. RT Raman spectrum of the 2 at.% Yb:Y_2O_3 ceramic fabricated using LiF sintering additive, numbers denote the Raman frequencies in cm^{-1}, λ_{exc} = 488 nm.

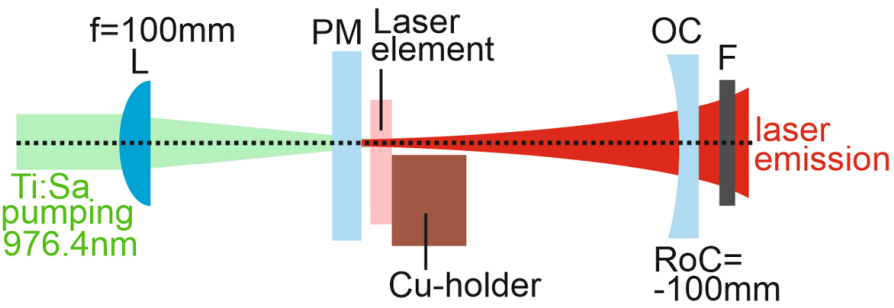

Figure 11. Scheme of the laser set-up: L – focusing lens, PM – pump mirror, OC – output coupler, F – long-pass filter.

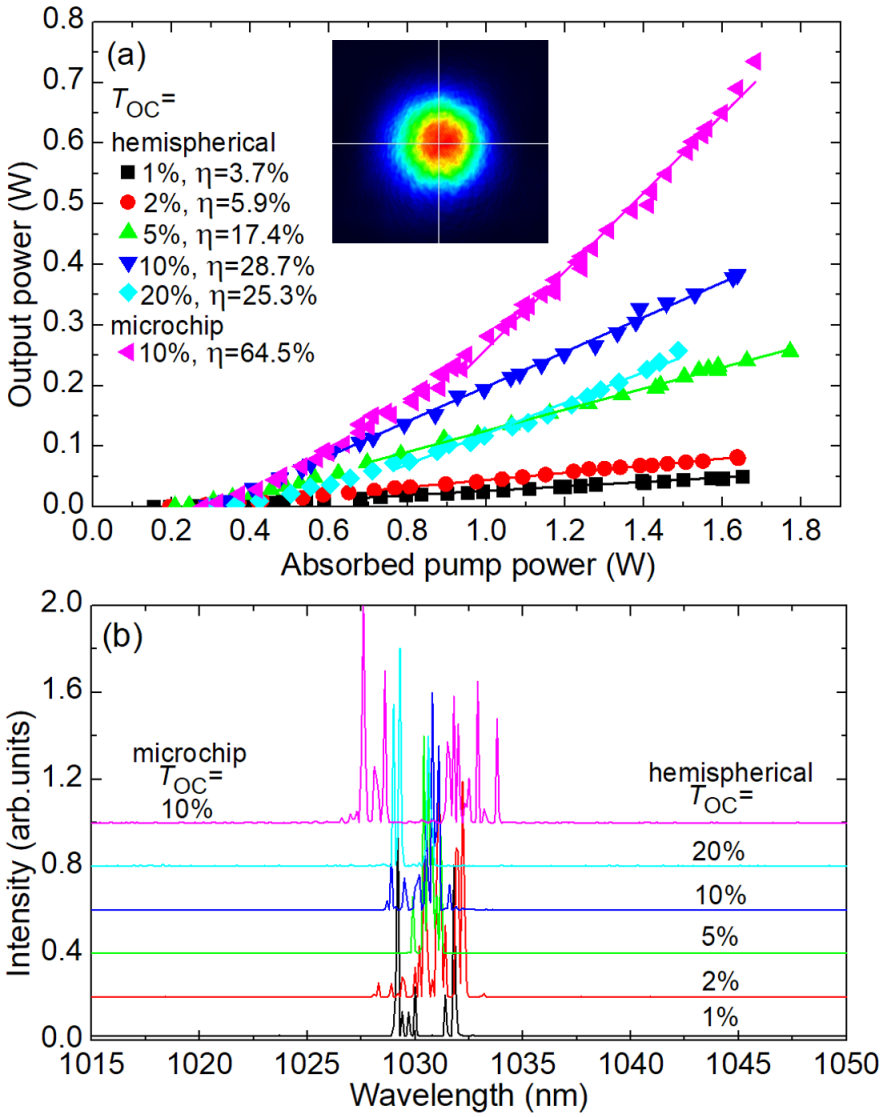

Figure 12. 2 at.% Yb:Y_2O_3 ceramic laser: (a) input-output dependences, η – slope efficiency, *inset* – typical profile of the laser mode in the far-field, hemispherical cavity, T_{OC} = 10%, P_{abs} ~1.0 W; (b) spectra of the laser emission at an absorbed pump power of 1.2 W, λ_P = 976.4 nm.

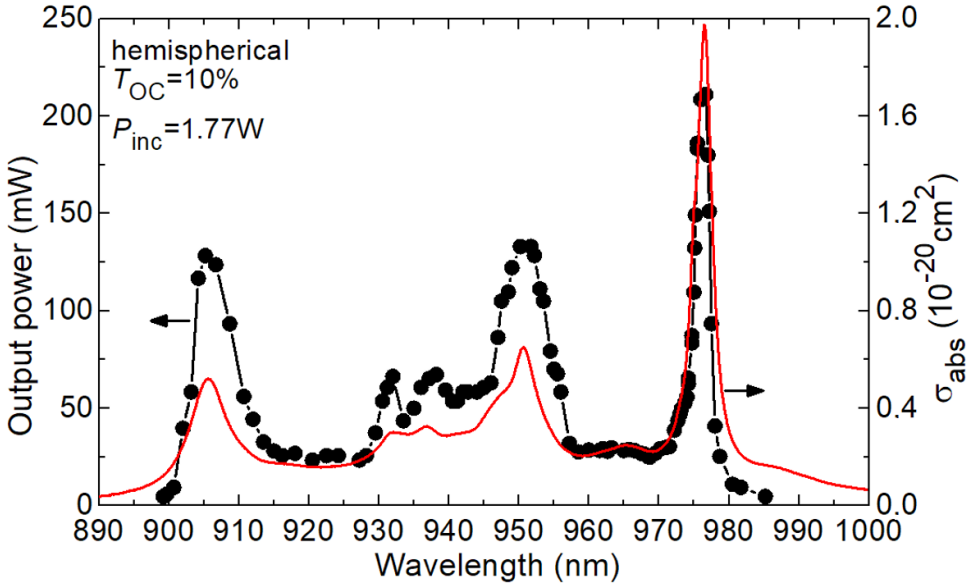

Figure 13. Laser excitation curve (output power vs. the pump wavelength) for the 2 at.% Yb:Y_2O_3 ceramic laser, T_{OC} = 10%, P_{inc} = 1.77 W. The σ_{abs} spectrum for Yb^{3+} ions is shown for comparison.